

MDPI

Article

Conformational, Electrochemical, and Antioxidative Properties of Conjugates of Different Ferrocene Turn-Inducing Scaffolds with Hydrophobic Amino Acids

Monika Kovačević ^{1,*} , Sunčica Roca ^{2,*} , Dijana Jadreško ³ , Jasna Mrvčić ⁴ , Karla Hanousek Čiča ⁴, Mojca Čakić Semenčić ¹ and Lidija Barišić ¹

- Department of Chemistry and Biochemistry, Faculty of Food Technology and Biotechnology, University of Zagreb, Pierottijeva 6, 10000 Zagreb, Croatia; mojca.cakic@pbf.unizg.hr (M.Č.S.); lidija.barisic@pbf.unizg.hr (L.B.)
- NMR Centre, Ruđer Bošković Institute, Bijenička 54, 10000 Zagreb, Croatia
- Laboratory for Physical Chemistry of Traces, Division for Marine and Environmental Research, Ruder Bošković Institute, Bijenička 54, 10000 Zagreb, Croatia; djadresko@irb.hr
- Department of Food Engineering, Faculty of Food Technology and Biotechnology, University of Zagreb, Pierottijeva 6, 10000 Zagreb, Croatia; jasna.mrvcic@pbf.unizg.hr (J.M.); karla.hanousek.cica@pbf.unizg.hr (K.H.Č.)
- * Correspondence: monika.kovacevic@pbf.unizg.hr (M.K.); sroca@irb.hr (S.R.); Tel.: +385-1-4605-275 (M.K.); +385-1-4571-224 (S.R.)

Abstract: The incorporation of different ferrocene scaffolds into the peptide sequences induces the formation of hydrogen-bond-based secondary structural elements that are frequently observed in natural peptides and proteins. There are three simple ferrocene scaffolds for conjugation with amino acids and peptides that serve as templates for ferrocene peptidomimetics, namely ferrocene-1,1'-dicarboxylic acid (Fcd, I), 1'-aminoferrocene-1-carboxylic acid (Fca, III), and ferrocene-1,1'-diamine (Fcda, V). Here, we have investigated their ability to induce the turn structure upon conjugation with Val, Leu, and Phe. Furthermore, we also wanted to determine whether the branched side chains of Val, Leu, and Phe interfere with intramolecular hydrogen bonding (IHB). For these purposes, we performed a detailed spectroscopic analysis by measuring the concentration, temperature, and solvent dependence of the IR, NMR, and CD spectra. The effect of the different ferrocene scaffolds on the antioxidant activity of the prepared peptides was tested using the DPPH and ABTS methods, and was further rationalized using electrochemical measurements. It was found that the ferrocene scaffold has the greatest influence on the hydrogen bonding pattern, while the influence of the side branches of the amino acids is less relevant.

Keywords: ferrocene; peptidomimetics; antioxidant activity; valine; leucine; phenylalanine; conformational analysis; hydrogen bonds; cyclic voltammetry



Citation: Kovačević, M.; Roca, S.; Jadreško, D.; Mrvčić, J.; Hanousek Čiča, K.; Čakić Semenčić, M.; Barišić, L. Conformational, Electrochemical, and Antioxidative Properties of Conjugates of Different Ferrocene Turn-Inducing Scaffolds with Hydrophobic Amino Acids. *Inorganics* 2024, 12, 195. https://doi.org/ 10.3390/inorganics12070195

Academic Editor: Vladimir Arion

Received: 26 June 2024 Revised: 11 July 2024 Accepted: 12 July 2024 Published: 18 July 2024



Copyright: © 2024 by the authors. Licensee MDPI, Basel, Switzerland. This article is an open access article distributed under the terms and conditions of the Creative Commons Attribution (CC BY) license (https://creativecommons.org/licenses/by/4.0/).

1. Introduction

Since the conformational stability, biological activities, and therapeutic properties of peptides and proteins are related to their secondary structure, the main goal in the design and preparation of synthetic peptides is to enable the formation of secondary structure elements [1–4]. Ferrocene peptides are known for their ability to adopt the turn- and β -sheet-like structures, similar to those found in natural peptides, as a result of intramolecular hydrogen bonding [5–8].

Kraatz and Metzler-Nolte have established three different types of 1,n'-disubstituted peptide systems based on the parent compound [9]. Since the choice of the ferrocene scaffold (**I**, **III**, and **V**) dictates the orientation of the peptide chain and affects the rigidity of the molecule depending on the pattern of hydrogen bonds established, it is possible to prepare three types of ferrocene peptides, i.e.: **II**, **IV**, and **VI** (Figure 1).

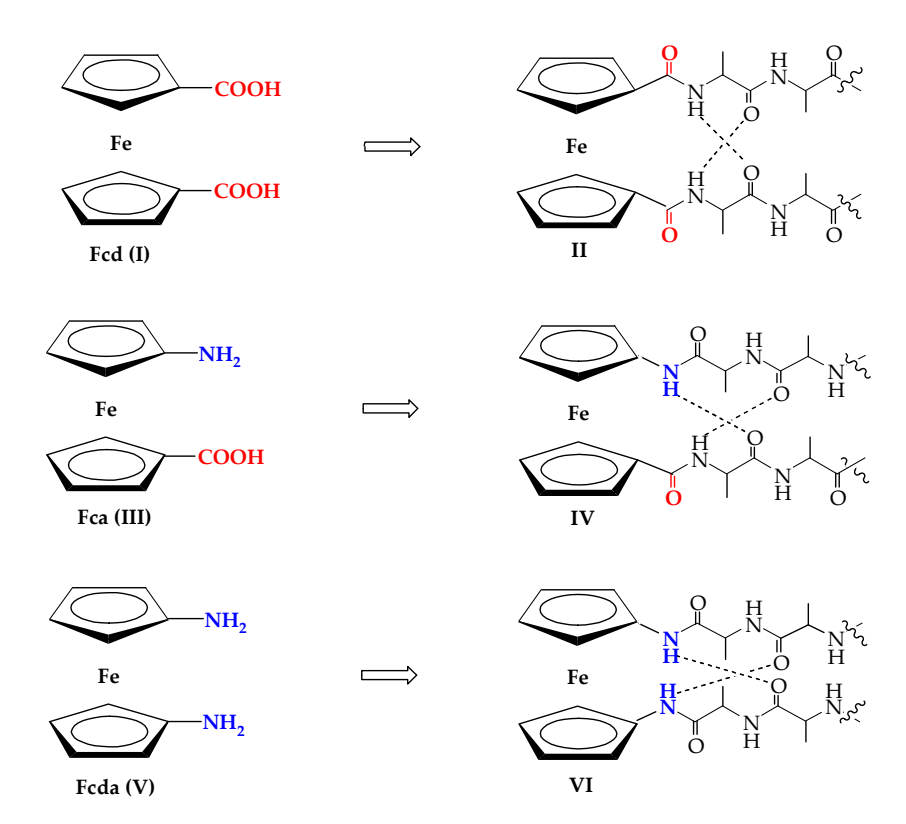


Figure 1. Ferrocene–alanine peptides **II**, **IV**, and **VI** derived from Fcd (**I**), Fca (**III**), and Fcda (**V**) (IHB denoted as dashed lines).

For example, amino acid or peptide conjugates II derived from the Fcd (I) most commonly form intramolecular interchain hydrogen bonds that form two ten-membered rings (two β -turns) in the resulting C_2 -symmetric peptide structure. (Figure 1). This structural motif is known as the 'Herrick' conformation. Alternative motifs are less frequently observed, such as the structure with only one interchain IHB closing the seven-membered γ -turn ring, the so-called 'van Staveren's' conformation or 'Xu's' open conformation, in which no intramolecular hydrogen bonding interactions occur [10–13].

The essential feature of Fca (III) is that, in contrast to Fcd (I) and Fcda (V), it enables the formation of a 12-membered IHB ring between antiparallel podand peptide chains, as found in natural peptides [14–17].

Compared to peptides II and IV, conjugates derived from ferrocene-1,1'-diamine (V) have been less studied [5,18–20]. The formation of 14-membered IHB rings between podand peptide chains, similar to those in antiparallel β -sheets, makes it a desirable structural element.

It has been shown that isosteric modification of bioactive compounds with ferrocene enhances antimicrobial, antioxidant, and anticancer activity due to the exceptional properties of ferrocene, e.g., superaromaticity, air and heat stability, electrophilicity, solubility in organic solvents, non-toxicity, and lipophilicity [21–24]. Therefore, the biological potential of the new peptides **1–9** is also being investigated.

Peptide sequences containing a high number of amino acids with hydrophobic side chains, so-called β -branched amino acids (Leu, Val, Phe, or Ile), are known to form β -sheet or α -helical structures supported by strong inter- or intramolecular non-covalent interactions [25].

Mitochondria-penetrating peptides (MPPs), a subclass of cell-penetrating peptides (CPPs), are short amino acid sequences that are able to penetrate the plasma membrane, i.e., the mitochondrial lipid bilayer. This is facilitated by the hydrophobic residues of the hydrophobic amino acids, which provide a high degree of lipophilicity [26]. It is known

that hydrophobic interactions cause the folding of proteins and stabilize the structures of single proteins, multiproteins, and protein—ligand systems [27].

The presence of hydrophobic amino acids in naturally occurring or synthetically produced antimicrobial peptides (AMPs) facilitates their distribution in microbial membranes [28]. Saint Jean et al. used the peptide C18G as a model system in which peptide variants were synthesized by replacing Leu residues with other hydrophobic amino acids and 2-aminoisobutyric acid. This led to the conclusion that hydrophobic groups in the AMP sequence play an important role in binding and the ability of the peptide to exhibit antibacterial activity. Therefore, controlling the hydrophobic groups in AMPs could be an approach to tune the activity to an optimal therapeutic window [29].

The study on the relationship between structure and antioxidant activity has shown that the antioxidant capacity of peptides is closely related to some structural features such as molecular mass, amino acid composition, sequences, and hydrophobicity [30]. A higher content of hydrophobic amino acids compared to hydrophilic amino acids was found in peptides with high antioxidant activity, which is considered to be a key factor for the radical scavenging ability of peptides [31,32]. The groups of Chanput and Li investigated the QSAR (Quantitative Structure–Activity Relationships) concept for antioxidant peptides, and more specifically the antioxidant activities of tripeptide libraries against the peroxidation of linoleic acid. Chanput et al. pointed out that hydrophobic amino acids such as Ile, Leu, Phe, Trp, Tyr, and Val are required for the antioxidant activity of peptide segments [33], while Li et al. showed that the *N*-terminal amino acid should be a highly hydrophobic amino acid (such as Ala, Gly, Val, and Leu), while the middle amino acid should have high hydrogen-bonding ability (such as basic Arg, Lys, and His) [34,35].

The work of Ohashi et al. discussed the correlation between six different antioxidant assays in the structure–activity relationship of antioxidant peptides based on the free radical scavenging activities of two series of tripeptide libraries [36]. The highest superoxide radical and reducing power activities were shown in the nanofiltrat fraction (1–4 kDa) from dark tuna muscle by-products containing antioxidant amino acids such as Tyr, Phe, Pro, Ala, His, and Leu, as reported by Saidi [37].

Ferrocene dipeptides derived from Fca (III) and hydrophobic amino acids (Phe, Val, and Leu) showed antimicrobial and antioxidant activity as well as high resistance to proteolytic cleavage, suggesting that the ferrocene scaffold plays an important role in stabilizing the dipeptides against enzymatic degradation [38]. In the same study, we have determined that the chirality of the amino acid groups, polarity of the protecting groups, and hydrophobicity influence the antimicrobial and antioxidant activity of the compounds due to the different patterns of hydrogen bonds formed. In recent research, derivatives of Fcda ($\bf V$) and various hydrophobic amino acids ($\bf L$ -/ $\bf D$ -Val, $\bf L$ -/ $\bf D$ -Leu, and $\bf L$ -/ $\bf D$ -Phe) were prepared to investigate whether Fcda induces a $\bf \beta$ -turn upon conjugation with an amino acid and whether the bulkiness of the Phe, Val, and Leu side-branches affects the pattern of hydrogen bonds [20].

In view of the previously mentioned results of the conformational analysis of ferrocene peptides, which point to the role of the ferrocene scaffold as a nucleator of turn-like structures, we decided to investigate the influence of the structurally different ferrocene scaffolds [Fcd (I), Fca (III), and Fcda (V)] (Figure 2) and the bulkiness of amino acid side chains on the conformational and electrochemical properties of bioconjugates II (1–3), IV (4–6), and VI (7–9) using IR, NMR, and CD spectroscopy, as well as cyclic voltammetry.

To determine how the aforementioned factors influence biological activity, the obtained compounds were analyzed for their antioxidative properties using the DPPH and ABTS methods. In addition, the obtained antioxidant activity of compounds **1–9** was further rationalized using electrochemical measurements. To the best of our knowledge, we have not found any examples in the literature dealing with the comparability of three types of ferrocene synthons and their influence on antioxidant activity.

Inorganics **2024**, 12, 195 4 of 18

 $[Ra = -CH(CH_3)_2, Rb = -CH_2CH(CH_3)_2, Rc = -CH_2Ph]$

Figure 2. Symmetrically disubstituted ferrocene peptides II, IV, and VI.

2. Results and Discussion

All spectroscopic measurements related to conformational analysis can be found in the Supplementary Materials. Although the synthesis of the target compounds has already been described in previous publications [6,16,20,39,40], we repeated all IR, NMR, and CD measurements to ensure the same conditions and reliable correlation.

2.1. Infrared Spectroscopy (IR Spectroscopy)

Infrared spectroscopy (IR) is an instrumental method that measures the wavelength and intensity of the absorption of infrared radiation and provides a reliable insight into the conformational space of peptides in a solution, based on NH and CO absorptions [41]. Stretching frequencies above 3400 cm⁻¹ are attributed to free NH groups, while NH bands below 3400 cm⁻¹ indicate their involvement in hydrogen bonding (Table 1, Figure 3). Absorption bands of carbonyl ester groups were detected below 1730 cm⁻¹, also indicating their involvement in hydrogen bonding [42].

In dichloromethane solutions of tripeptides **1–9** ($c = 5 \times 10^{-2}$ M), distinct signals were observed in the region of the NH stretching vibrations, with the signals of the associated NH dominating (<3400 cm⁻¹) (Table 1). The graph (Supplementary Materials Figure S1) showing the stretching vibrations in the region of the NH groups of the peptides prepared from Fcd (**I**) demonstrates that almost all NH groups are associated.

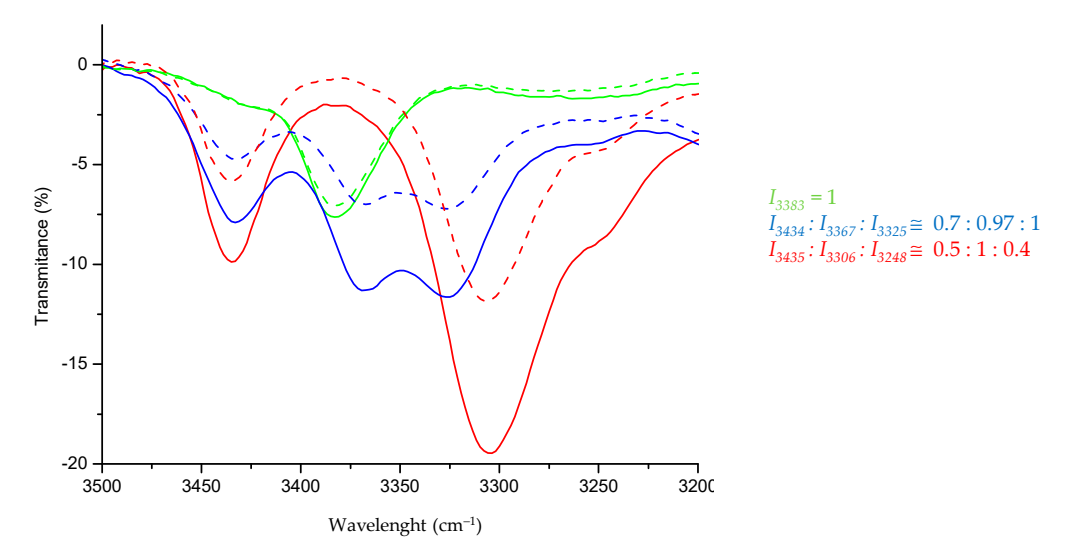


Figure 3. The NH stretching vibrations of **1** (—), **4** (—), and **7** (—) [$R_a = -CH(CH_3)_2$], in IR spectra [CH_2Cl_2 [(—) $c = 5 \times 10^{-2}$ M; (···) $c = 2.5 \times 10^{-2}$ M].

Inorganics **2024**, 12, 195 5 of 18

Compound	ν _{NH} (Free)	$ u_{ m NH} $ (Associated)	$ u_{\rm CO} $ (Ester)	
MeO-Val-CO-Fn *-CO-Val-OMe (1)	3430	3389	1729	
MeO-Leu-CO-Fn-CO-Leu-OMe (2)	3429	3372	1729	
$MeO-Phe-\overline{CO-Fn-CO}-Phe-OMe$ (3)	3434	3378	1730	
MeO-Val-CO-Fn-NH-Val-Boc (4)	3433	3369, 3326	1720	
MeO-Leu-CO-Fn-NH-Leu-Boc (5)	3434	3372, 3322	1724	
$MeO-Phe-\overline{CO-Fn-NH}-Phe-Boc$ (6)	3430	3375, 3326	1725	
Ac-Val-NH-Fn-NH-Val-Boc (7)	3422	3324	1710	
Ac-Leu-NH-Fn-NH-Leu-Boc (8)	3425	3320	1708	
$Ac-Phe-\overline{NH-Fn-NH}-Phe-Boc$ (9)	3416	3324	1709	

Table 1. Stretching frequencies [ν (cm⁻¹)] of NH and CO groups of 1–9 in CH₂Cl₂ ($c = 5 \times 10^{-2}$ M).

The ratio of the bonded and non-bonded NH groups in the IR spectra of peptides 1, 4, and 7, obtained by the conjugation of Val with ferrocene scaffolds I, III, and V, allows us to conclude which ferrocene scaffold favors the participation of NH groups in IHB (Figure 3). It can be seen that the formation of hydrogen bonds is most favored in the presence of Fcda (V) as the nucleating scaffold, since the proportion of the associated NH band is highest in peptide 7 (0.5:1). The lowest potential to induce IHBs is shown for the scaffold Fca (III), since the ratios of free and associated NH bands are 0.7:1.

Figure S1 shows that there is a pattern to how side-branching of the hydrophobic amino acids affects the intensity of the associated and free bands, as the ratio of free and associated NH bands shows that the bulky benzyl side chains strongly interfere with hydrogen bonding. In peptides III and V, the excessive ratio of free and associated NH bands (0.7:1 and 1:1) indicates a higher proportion of non-bonded states in conjugates 6 and 9, with phenylalanine compared to conjugates with valine (4 and 7) and leucine (5 and 8) (0.5:1 and 0.6:1).

To further characterize the inter- or intramolecular nature of hydrogen bonding (association), it is necessary to test the concentration-dependence of the IR spectra. With a gradual dilution of the solution of the tested sample, the intermolecular hydrogen bonds tend to cleave, resulting in a decrease in the intensity of the associated NH bands compared to those of the free NH groups. In contrast, when intramolecular hydrogen bonds are formed, the ratio of free and associated bands remains unchanged. Here, the concentration-independent IR spectra of peptides **1–9** indicate the intramolecular character of the hydrogen bonds (Supplementary Materials S3, S8, S13, S18, S23, S28, S33, S38, and S43).

2.2. Nuclear Magnetic Resonance Spectroscopy

Nuclear magnetic resonance (NMR) is a method that can be used not only to determine the chemical structure of molecules, but also to gain a better insight into the patterns of hydrogen bonding. This method can be applied to distinguish whether individual NH groups are involved in hydrogen bonds. Thus, if the signal of the NH group is downfield shifted (above 7 ppm), this group is involved in hydrogen bonding [43,44].

A common feature of conjugates **1–9** is a high chemical shift of the amide protons of the ferrocene scaffold (NH_{Fn}), indicating their involvement in hydrogen bonding. Considering that the NH protons of the *N*-protecting groups (NH_{Ac} and NH_{Boc}) are upfield shifted (δ < 7.0 ppm), they are not expected to be involved in IHBs (Table 2).

In peptides **1–3** (type **II**) with an amide bond between Val, Leu, or Phe, respectively, and a carbonyl group of the ferrocene scaffold (**I**), the NH signals are slightly upfield shifted (δ ~7.5–7.8 ppm) compared to peptides **IV** (**4–6**) and **VI** (**7–9**) (δ > 9.0 ppm), which originate from scaffolds **III** and **V** with an NH group bound to the ferrocene unit.

^{*} Fn = ferrocenylene.

Commound	δ (ppm)						
Compound	(NH _{CO})	(NH _{Fn} ^a)	(NH _{Fn} ^b)	(NH _{Ac})	(NH _{Boc})		
MeO-Val-CO-Fn-CO-Val-OMe (1)	7.49						
$MeO-Leu-\overline{CO-Fn-CO}-Leu-OMe$ (2)	7.76						
$MeO-Phe-\overline{CO-Fn-CO}-Phe-OMe$ (3)	7.72						
MeO-Val-CO-Fn-NH-Val-Boc (4)	7.5	9.01			5.11		
$MeO-Leu-\overline{CO-Fn-NH}-Leu-Boc$ (5)	7.62	9.33			5.01		
$MeO-Phe-\overline{CO-Fn-NH}-Phe-Boc$ (6)	7.5	8.98			5.20		
Ac-Val-NH-Fn-NH-Val-Boc (7)		9.21	9.04	6.75	5.21		
Ac-Leu-NH-Fn-NH-Leu-Boc (8)		9.38	9.16	7.3	5.16		
$Ac-Phe-\overline{NH-Fn-NH}-Phe-Boc$ (9)		9.16	9.1	6.9	5.34		

Table 2. Chemical shifts $[\delta/ppm]$ of the NH protons of **1–9** in CDCl₃-d ($c = 5 \times 10^{-2}$ M).

2.2.1. Concentration-Dependent NMR

Based on the concentration-independent IR specta, we assumed the intramolecular character of the hydrogen bonds in peptides II (1–3), IV (4–6), and VI (7–9), which has to be confirmed by examining the concentration-dependent 1H NMR spectra. However, it should be taken into account that the dilution or cleavage of intermolecular hydrogen bonds causes an upfield shift of the amide protons. As can be seen from the plots in Figure 4, the gradual decrease in CDCl₃-d concentration (from high-50 mM to low-6.25 mM) did not lead to significant changes in the chemical shifts of the NH_{Fn} protons, which is further confirmation of the intramolecular nature of the hydrogen bonds, as suggested using IR spectroscopy. Even though the concentration-independent IR spectra of peptides VI (7–9) exclude the presence of intermolecular hydrogen bonds, the significantly changed chemical shifts of the acetamide NH_{Ac} protons upon dilution ($\Delta\delta$ ~0.6–1 ppm) still indicate the possible presence of intermolecular aggregates (Figure 4c).

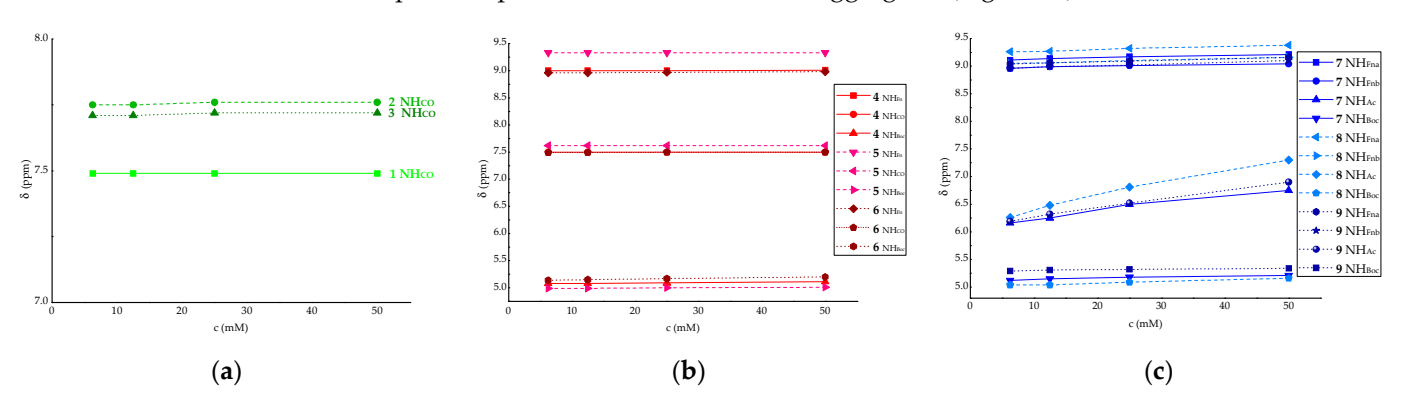


Figure 4. Concentration dependence of the amide proton chemical shifts for (a) 1–3, (b) 4–6 and (c) 7–9.

2.2.2. Temperature-Dependent NMR

To further confirm the intramolecular character of the hydrogen bonds in peptides II, IV, and VI, temperature-dependent imaging of a 12.5 mM peptide solution in CDCl₃-d in the range of 250–330 K was also performed (Figure 5). In our previous studies [17,18,20], we found that when peptide solutions are heated in the mentioned range, the chemical shifts of the free amide protons or those involved in the formation of IHB remain the same or change slightly, with the change in the proton shift range being up to 0.3 ppm. When amide protons are involved in intermolecular hydrogen bonding, the change in shift is more pronounced ($\Delta\delta$ ~1–4 ppm).

 $^{^{}a,b}$ = denoted on Figure 2.

From the plots of the temperature dependence of peptide II (1–3), it is evident that the change in the chemical shift of NH is insignificant ($\Delta\delta$ < 0.4 ppm), regardless of the constituent amino acid, thus confirming the intramolecular character of the hydrogen bonds in this type of peptide. The same difference in the displacement of amide protons is evident from the temperature dependence diagram of type IV (4–6) peptides. Considering that the signals of NH_{Fn} in peptides VI (7–9) have smaller upfield shifts ($\Delta\delta$ < 0.6 ppm), it is confirmed that they are involved in strong IHBs. At the same time, the larger upfield shifts ($\Delta\delta$ > 1.2 ppm) experienced by NH_{Ac} in dipeptides 8 and 9 are certainly due to their involvement in less stable structures.

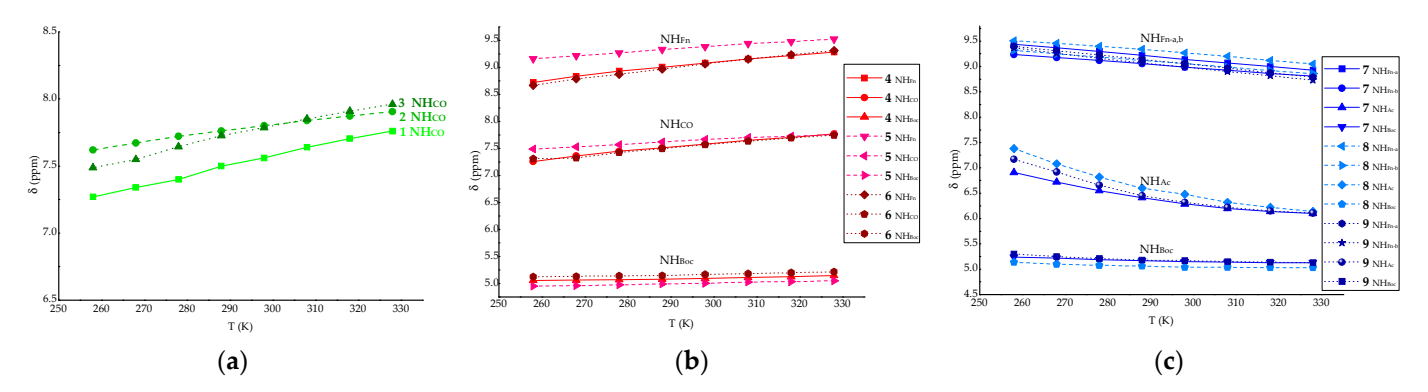


Figure 5. Temperature dependence of the amide proton chemical shifts for (a) 1–3, (b) 4–6, and (c) 7–9.

Intermolecular hydrogen bonds, as well as hydrogen bonds with the solvent, are cleaved at an elevated temperature, which leads to an upfield shift in the NH group signal. In other words, the dependence on low temperatures in CDCl₃ is due to exposed and shielded NH groups, while the dependence on high temperatures always indicates NH groups that were shielded at the beginning of the measurement but which were exposed to the solvent upon heating due to dissociation of self-assembled aggregates or dissolution of the ordered conformation. The exposure of the NH groups of the peptides to the solvent is determined by the dependence of the chemical shifts on the temperature, the temperature coefficients ($\Delta\delta/\Delta T$). Larger values correspond to the initially shielded protons (involved in hydrogen bonding) exposed to the solvent during the unfolding of IHB-stabilized structures or the dissociation of aggregates at higher temperatures [45-48]. Therefore, the concentration-independent NH_{Fn} and NH_{CO} show larger temperature coefficients $(-3.85 \text{ to } -9.28 \text{ ppb K}^{-1})$, confirming their involvement in IHB-mediated folding. The large temperature coefficients (-11.57 to -17.71 ppb K⁻¹) of NH_{Ac} further confirms their involvement in self-assembly. Nevertheless, NH_{Boc} shows no significant dependence on temperature as it is not involved in HBs (Table 3).

Thus, the increased temperature dependencies of the chemical shifts of ferrocene peptides **II**, **IV**, and **VI**, which have been shown to be independent of concentration (ruling out the possibility of their intermolecular aggregations), reflect the originally shielded NH groups being exposed to the solvent by breaking the conformations ordered by intramolecular hydrogen bonds.

Commound	$\Delta\delta/\Delta T$ (ppb K $^{-1}$)						
Compound	(NH _{CO})	(NH _{Fn} ^a)	(NH _{Fn} ^b)	(NH _{Ac})	(NH _{Boc})		
MeO-Val-CO-Fn-CO-Val-OMe (1)	-7						
$MeO-Leu-\overline{CO-Fn-CO}-Leu-OMe$ (2)	-4.22						
MeO-Phe-CO-Fn-CO-Phe-OMe (3)	-6.11						
MeO-Val-CO-Fn-NH-Val-Boc (4)	-7.14	-8			-1.28		
MeO-Leu- <u>CO-Fn-NH</u> -Leu-Boc (5)	-3.85	-5.28			-1.42		
MeO-Phe-CO-Fn-NH-Phe-Boc (6)	-6.28	-9.28			-1.28		
Ac-Val-NH-Fn-NH-Val-Boc (7)		-7.28	-6.14	-11.57	-1.57		
Ac-Leu-NH-Fn-NH-Leu-Boc (8)		-6.57	-6.57	-17.71	-1.57		
$Ac-Phe-\overline{NH-Fn-NH}-Phe-Boc$ (9)		-8.71	-9.14	-15.14	-2.42		

Table 3. Temperature coefficients ($\Delta \delta/\Delta T$) of the NH protons **1–9** in CDCl₃-d ($c = 5 \times 10^{-2}$ M).

2.2.3. Solvent-Dependence of NMR Chemical Shifts

The strength of the IHBs resulting from the IR and NMR data presented above was tested using titration with DMSO- d_6 . While a significant downfield shift of the NH protons exposed to polar DMSO- d_6 is expected, the NH protons involved in strong hydrogen bonds are shielded from DMSO, and their chemical shifts remain almost unchanged [49,50]. It was found that titration of 12.5 mM CDCl₃-d solutions of peptides II, IV, and VI with DMSO- d_6 significantly affected the chemical shifts of the NH protons of MeO-Phe-CO-Fn-CO-Phe-OMe (3) and the NH_{Ac/Boc} protons in peptides IV (4–6) and VI (7–9) ($\Delta\delta$ > 0.6 ppm), indicating their involvement in weak IHBs. In contrast, no change in chemical shift was observed for the downfield-shifted NH protons of the ferrocene scaffolds upon addition of DMSO- d_6 , confirming their involvement in strong IHBs (Figure 6).

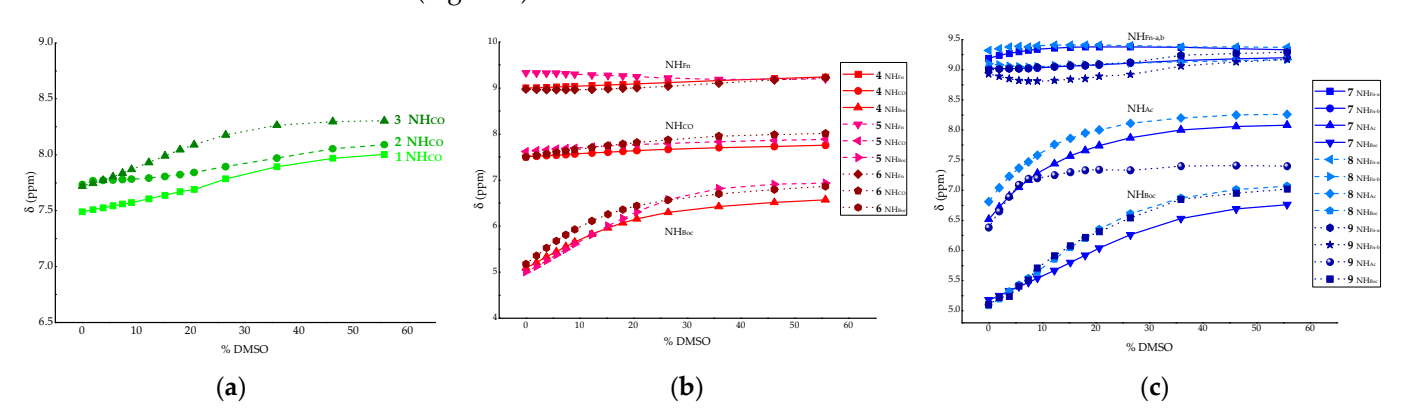


Figure 6. Solvent dependence of the amide proton chemical shifts of (a) 1-3, (b) 4-6, and (c) 7-9.

2.3. Circular Dichroism (CD)

Circular dichroism (CD) is a spectroscopic method that enables the determination of secondary structure elements in chiral peptides. When a ferrocene scaffold is introduced into the chiral peptide environment to induce the formation of turn- and β -sheet-like structures, the free rotation of the ferrocene rings is disabled, resulting in the helical chirality of the ferrocene core, and the strong Cotton effect is observed in the ferrocene chromophore region (λ ~480 nm) [51]. The sign of the Cotton effect is influenced by the protecting groups, the solvent and the type and sequence of the bound natural amino acids [52–54].

As shown in Table 4 and in Supplementary Materials S2, peptides **1–9**, which contain different ferrocene turn-inducing scaffolds, show positive Cotton effects.

 $^{^{}a,b}$ = denoted on Figure 2.

Inorganics 2024, 12, 195 9 of 18

Ac-Phe-NH-Fn-NH-Phe-Boc (9)

Commound	$[heta]$ /deg cm 2 dmol $^{-1}$			
Compound	CH ₂ Cl ₂	CH ₂ Cl ₂ +DMSO		
MeO-Val-CO-Fn-CO-Val-OMe (1)	4449	3779		
$MeO-Leu-\overline{CO-Fn-CO}-Leu-OMe$ (2)	5595	5032		
$MeO-Phe-\overline{CO-Fn-CO}-Phe-OMe$ (3)	2683	2577		
MeO-Val-CO-Fn-NH-Val-Boc (4)	9923	5364		
$MeO-Leu-\overline{CO-Fn-NH}-Leu-Boc$ (5)	10515	8530		
$MeO-Phe-\overline{CO-Fn-NH}-Phe-Boc$ (6)	6663	3284		
Ac-Val-NH-Fn-NH-Val-Boc (7)	25,958	21,125		
Ac-Leu-NH-Fn-NH-Leu-Boc (8)	21,828	18,709		

Table 4. Cotton effects $\{[\theta]/\deg \text{cm}^2 \text{dmol}^{-1}\}\$ of **1–9** in CH₂Cl₂ $(c = 5 \times 10^{-2} \text{ M})$ and upon addition of 20% DMSO.

Peptides VI (7-9) with ferrocene diamine scaffold (NH-Fn-NH), which were involved in stronger IHBs, also have significantly higher Cotton effects than peptides IV (4-6) with a CO-Fn-NH scaffold and II (1-3) with a CO-Fn-CO scaffold. Therefore, ferrocene diamine was found to induce the formation of the most stable chirally ordered structures among the three tested scaffolds.

15,001

10,994

In addition, a titration of 5 mM CH₂CL₂ solution with DMSO as a competing solvent was performed to test the stability of the folded structures. If the highly ordered structures are adopted, the addition of DMSO will not noticeably affect the intensity of the Cotton effect. As expected, the addition of 20% DMSO caused an attenuation of the Cotton effect by up to 50% for type IV peptides (4–6), and a less pronounced attenuation for type II (1–3) and type VI peptides (7–9) (Table 3, Figure 7).

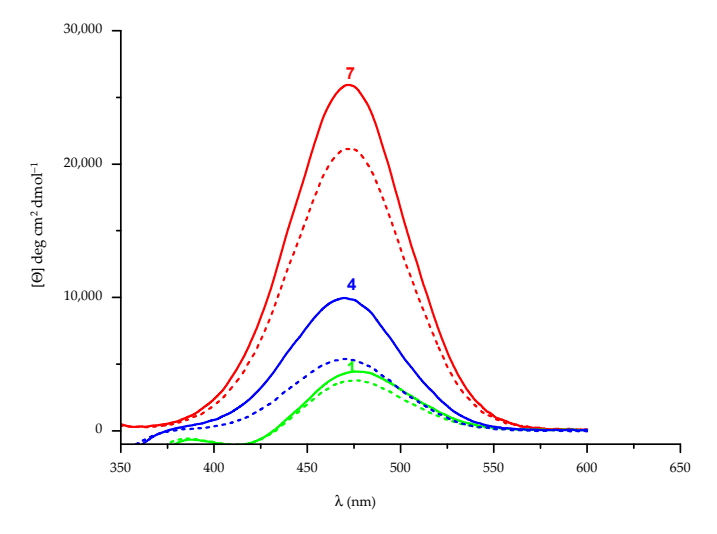


Figure 7. The Cotton effects in chirality-organized ferrocene peptides 1 (green), 4 (blue), and 7 (red) in solution { $CH_2Cl_2[(-)c = 5 \times 10^{-3} \text{ M})$ }, $CH_2Cl_2(c = 5 \times 10^{-3} \text{ M})$ containing 20% of DMSO (···)}.

2.4. Antioxidant Activity

The antiradical activity of the tested ferrocene compounds (1–9) was estimated using assays to determine the compounds' ability to scavenge the following free radicals: 2'diphenyl-1-picrylhydrazyl radical (DPPH), and 2,2'-azinobis(3-ethylbenzothiazoline-6sulfonate) cationic radical (ABTS). The results of radical scavenging activity of the tested compounds at a concentration of 1 mM, expressed as mM Trolox equivalents, are shown in Table 5.

Table 5. Antioxidant activity of ferrocene peptides evaluated using a 1,1-diphenyl-2-picryl-hydrazyl radical scavenging assay (DPPH) and 2,2'-azinobis(3-ethylbenzothiazoline-6-sulfonate) cationic radical scavenging assay (ABTS) of **1–9** ($c = 1 \times 10^{-3}$ M).

Commound	mM Trolx			
Compound	DPPH	ABTS		
MeO-Val-CO-Fn-CO-Val-OMe (1)	0.047 ± 0.012	0.248 ± 0.093		
MeO-Leu-CO-Fn-CO-Leu-OMe (2)	0.034 ± 0.019	0.137 ± 0.017		
$MeO-Phe-\overline{CO-Fn-CO}-Phe-OMe$ (3)	0.050 ± 0.010	0.114 ± 0.017		
$MeO-Val-\overline{CO-Fn-NH}-Val-Boc$ (4)	0.009 ± 0.001	1.651 ± 0.090		
MeO-Leu-CO-Fn-NH-Leu-Boc (5)	0.008 ± 0.008	0.813 ± 0.036		
$MeO-Phe-\overline{CO-Fn-NH}-Phe-Boc$ (6)	0.007 ± 0.000	1.147 ± 0.067		
Ac-Val-NH-Fn-NH-Val-Boc (7)	0.026 ± 0.001	0.492 ± 0.024		
Ac-Leu-NH-Fn-NH-Leu-Boc (8)	0.043 ± 0.021	0.878 ± 0.000		
$Ac-Phe-\underline{NH-Fn-NH}-Phe-Boc$ (9)	0.028 ± 0.005	1.4617 ± 0.064		

The ferrocene compounds tested showed better scavenging activity against ABTS radicals than against DPPH radicals at the same concentration. This is consistent with the literature data suggesting that ferrocene derivatives may be more active in reducing radicals (such as ABTS-+) than in donating electrons or hydrogen atoms to N-centered radicals (such as DPPH') [55], whose steric accessibility is critical for antioxidant compounds [56]. Of all the compounds tested, MeO-Phe-CO-Fn-CO-Phe-OMe (3) had the highest antioxidant activity, as determined using the DPPH method, having the same range as MeO-Val-CO-Fn-CO-Val-OMe (1) and Ac-Leu-NH-Fn-NH-Leu-Boc (8). The weakest antioxidant activity is exhibited by group IV peptides (4-6). Contrary, this peptide class, with -CO-Fn-NH- scaffold shows the best antioxidant activity as determined by the ABTS method. The next group by antioxidant activity is derived from the ferrocene scaffold -NH-Fn-NH- (7-9), while the peptides with the scaffold -CO-Fn-CO- (1-3) show the weakest antioxidant activity.

Our previous work has shown that peptides derived from Fca (CO-Fn-NH) and Fcda (NH-Fn-NH) have moderate antioxidant activity in the range of 0.1 mM Trolox equivalent as determined using the DPPH method. It is hypothesized that oxidative stress due to abnormal levels of reactive oxygen species (ROS) is involved in the process of carcinogenesis. Highly reactive intermediates of biological oxidation processes interact with intracellular structures such as proteins, nucleic acids, lipids, and membranes and cause their oxidative damage. For this reason, there has recently been an increasing interest in the synthesis and evaluation of various structures, including metal complexes, derived from different metals and organic ligands that serve as protection against oxidative stress. The use of ferrocene as an antioxidant described in alarming detail. Milaeva et al. focused on metal-based antioxidants (2,6-dialkylphenols, flavonoids, polyphenols, N-containing heterocycles, and macrocyclic compounds) and their in vitro and in vivo activities in cellular oxidation processes [57]. Obviously, the extent of activity of the tested compounds depends on their molecular structures. Liu presented his ongoing studies on antioxidants with ferrocene. He found that the ferrocene moiety can enhance the antioxidant effect even without the phenolic hydroxyl group [58]. The role of ferrocene in enhancing the antioxidant effect could be due to the fact that it scavenges radicals, reduces the oxidative potential, and increases the affinity to the DNA strand. Minić Jančić et al. determined the antioxidant activity of ferrocenes containing a six-membered cyclic urea ring using the following two methods: ABTS radical cation, and DPPH radical scavenging activity. They concluded that some of the synthesized ferrocenyl derivatives possess strong ABTS-+ scavenging activity [59]. Tabrizi et al. prepared the conjugates of aminoferrocene with caffeic acid (CA) and ferulic acid (FA). The evaluation of radical scavenging activity of these conjugates and their ligands towards DPPH-, superoxide anion $(O_2^-$ -), NO-, and ABTS-+ using UV-VIS and electron spin resonance spectroscopy as well as DFT showed the higher antioxidant properties of aminoferrocene conjugates compared to their ligands [60]. These results

indicate that the ferrocene moiety is crucial for the results of antioxidant activity and that its redox potential changes effectively depending on the Fn-CO or Fn-NH binding mode with amino acids and peptides, as expected based on the electron donor/acceptor ability of the N-H and C=O groups, the hydrogen bonding network, and the dipole moment orientation [61,62].

2.5. Electrochemical Study

Voltametric techniques have been successfully used to investigate redox reactions of many bioactive compounds, since they can mimic the redox mechanisms of organisms *in vitro* [63–66]. Therefore, taking into account the obtained biological/antiradical activity, compounds **1–9** were further evaluated for their electron transfer properties, using cyclic (CV) voltammetry at a glassy carbon (GC) electrode. Accordingly, it was expected that information on the electrochemical mechanisms of the investigated compounds, as well as on the influence of different substituents on redox potentials, would give better insight into their physiological mechanisms of action and provide new information on the structure–electrochemical–antioxidant activity relations.

The electrochemical properties of 1–9 were investigated using cyclic voltammetry in (0.1 M Et₄NClO₄) acetonitrile solution using GC as a working electrode. Figure 8 shows cyclic voltammograms for the oxidation of three groups of ferrocene derivatives (1-3, 4-6, and 7-9) recorded at a scan rate of 100 mV s⁻¹, within the potential range from -0.6 to 1.4 V. Cyclic voltammetry measurements showed that compounds 1-3 and 4-6 provide a similar voltametric response, i.e., it consists of one pair of redox peaks (A1/C1) at about $E_{1/2} = 0.4 \text{ V}$ and $E_{1/2} = 0.2 \text{ V}$, respectively. These peaks correspond to the reversible charge transfer reaction of the ferrocene fragment on the GC electrode: $[Fe^{II}(C_5H_5)_2] \rightleftharpoons$ $[\text{Fe}^{\text{III}}(C_5H_5)_2] + e^-$ [67–70]. The difference in peak potentials is due to the structural differences between the two groups of studied compounds, i.e., the presence of different substituents on the ferrocene core. More specifically, the presence of -CO-Fn-NHscaffold in 4-6 causes a cathodic shift of the redox potential of peaks A1/C1, i.e., the electrochemical oxidation of ferrocene occurs at 250 mV more negative potential compared to compounds 1-3 as a result of the stronger electron-donating effect of -NH- group on Fc core, indicating lower energy required for primary electron transfer. On the other hand, a somewhat different electrochemical behavior was observed for compounds 7-9 under otherwise identical conditions (see Figure 8c). For these compounds, the redox potential of ferrocene shifts to more negative values by an additional 250 mV (relative to 4-6) due to the presence of -NH-Fn-NH- scaffold, i.e., an additional electron-donating -NH- group on the ferrocene core. Moreover, besides the cathodic shift of the Fc redox potential, the voltammograms of 7-9 show two new oxidation peaks A2 and A3 at potentials around 0.9 V and 1.1 V, respectively. According to the literature [71], these anodic peaks probably correspond to the irreversible one-electron oxidation of the secondary amine, giving a radical cation, followed by a chemical reaction giving electro-inactive products. However, a deeper insight into the origin of these oxidation peaks and their identification are not the subject of this study.

Finally, these observations are somewhat consistent with the observed antioxidant properties of 1–9, and support the fact that compounds with lower oxidation potential are more efficient radical scavengers. However, although it was expected that compounds 7–9 with the lowest oxidation potential would exhibit the strongest antioxidant activity, this was not the case. The most effective ABTS⁺ radical quenchers were peptides with the -CO–Fn–NH- scaffold, i.e., those with moderately low oxidation potential. This phenomenon can be explained by the fact that the antioxidant action of investigated compounds towards ABTS⁺ radicals may involve either electron (ET) or hydrogen atom transfer (HAT) (or both), and not exclusively the transfer of electrons. In other words, the oxidation potentials of investigated compounds were found to be more sensitive to the ferrocene scaffolds into the peptide sequences, which leads to a relative discrepancy between the scavenging activity and oxidation potential.

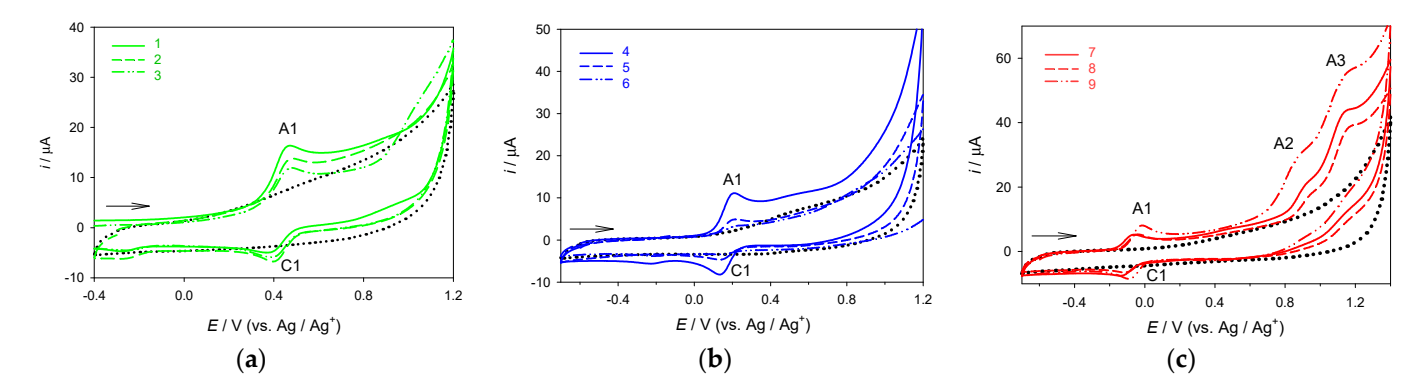


Figure 8. Cyclic voltammograms of 0.5 mmol/L solutions of (a) 1–3, (b) 4–6 and (c) 7–9 on GC electrode, in CH₃CN (0.1 M Et₄NClO₄). The scan rate was 100 mV s⁻¹. Dotted (black) lines represent cyclic voltammograms of the supporting electrolyte; the arrows indicate the scan direction.

The electrochemical (CV) peak potentials for the investigated compounds taken at the scan rate of 100 mV s^{-1} are shown in Table 6.

Table 6. The values of oxidation (A1, A2, and A3) and reduction (C1) CV peak potentials of compounds **1–9** in CH₃CN (0.1 mol/L Et₄NClO₄) on GC electrode. The scan rate was 100 mV s⁻¹.

Compound	1	2	3	4	5	6	7	8	9
<i>E</i> _p , A1/V	0.45	0.47	0.47	0.20	0.20	0.21	-0.07	-0.04	-0.02
$E_{\rm p}$, C1/V	0.39	0.40	0.40	0.14	0.14	0.15	-0.13	-0.10	-0.08
$E_{\rm p}$, A2/V	-	-	-	-	-	-	0.93	0.95	0.86
$E_{\rm p}$, A3/V	-	-	-	-	-	-	1.13	1.16	1.11

3. Materials and Methods

The IR spectra of the samples were recorded with a Perkin-Elmer Spectrum Two spectrophotometer as CH_2Cl_2 (Acros Organics, 99.5% for spectroscopy) solutions between NaCl windows. The concentration-dependent recording of the IR spectrum is also carried out using the stepwise binary dilution of a 50 mM ferrocene peptide solution in di-chloromethane.

 1 H and 13 C NMR spectra were recorded in CDCl₃- 2 d (Euristop, Paris, France, 99.80% D) or DMSO- 2 d (Euristop, Paris, France, 99.80% D), each with tetramethylsilane (TMS, $\delta = 0.0$ ppm) as internal standard, using a Bruker AV600 spectrometer (Bruker BioSpin GmbH, Rheinstetten, Germany) at the Ruđer Bošković Institute A 5 mm broadband probe head with z-gradient coils operating at 600.130 MHz for 1 H and 150.903 MHz for 13 C was used. Concentration-dependent spectra are recorded by diluting the initial 50 mM peptide solution in chloroform, and the temperature-dependent spectra involve recording a 25 mM peptide solution in chloroform at 8 different temperatures (258–328 K).

NMR titration is performed by adding 10 μ L DMSO- d_6 to a 25 mM peptide solution in CDCl₃-d. The spectra are recorded after each addition of DMSO- d_6 until the chemical shift of the observed NH groups no longer changes. When using CDCl₃-d/DMSO- d_6 mixture, calibration was performed using TMS as an internal standard.

CD spectra were recorded using a Jasco-810 spectropolarimeter in CH₂Cl₂ (Acros Organics, 99.5% for spectroscopy). Molar ellipticity coefficients (θ) are in degrees, concentration c is in molL⁻¹, and path length l is in cm, so the unit for (θ) is deg cm² dmol⁻¹. The CD activity of the peptides is investigated in the region of the ferrocene chromophore (λ ~480 nm). For this purpose, a 5 mM solution of the peptide is taken up in dichloromethane, and 20% DMSO (Supelco, Darmstadt, Germany, >99.8% for spectroscopy Uvasol[®]) is added to the same sample. The strength of the Cotton effect before and after the addition of DMSO is examined, and the attenuation of the signal strength is used to draw conclusions about the chiral arrangement of the peptides produced in the solution.

Regarding the DPPH assay, the antiradical activity of ferrocene compounds (concentration of 1 mM) against DPPH (1,1-diphenyl-2-picrylhydrazyl) (Fluka, Buchs, Switzerland, >85%) radicals was measured according to the method of Brand-Williams et al. [72]. Samples (250 $\mu L)$ were mixed with 0.1 mM DPPH working solution (2 mL). Absorbance at 517 nm was measured with a spectrophotometer after 30 min of incubation in the dark. Ethanol (Kemika, Zagreb, Croatia, p.a.) was used as a control. A calibration curve was constructed using Trolox as the reference antioxidant in the range of 0.01–0.05 mM (R2 = 0.9999). Results were expressed as millimoles Trolox equivalents (mM Trolox equivalents). Measurements were performed in triplicate.

ABTS radical cation scavenging activity. The ABTS radical scavenging activity of the tested compounds was estimated according to the method of Re et al. [73]. ABTS·+ was generated in the reaction of 7 mM stock solution of ABTS [2,2'-azinobis-(3-ethylbenzothiazoline-6-sulfonic acid) diammonium salt] (Sigma Aldrich, Steinheim, Germany, >98 %) with 140 mM potassium persulfate (Fluka, >99 %), and the mixture was left in the dark at room temperature for 16 h before use. Then, the ABTS-+ working solution was prepared by diluting the previously prepared mixture with 96% (v/v) ethanol (Kemika, Zagreb, Croatia, p.a.) until an initial absorbance value of 0.70 \pm 0.02 at 734 nm was obtained. Briefly, 20 μ L of sample was added to 2 mL of ABTS-+ working solution and the absorbance at 734 nm was measured after 6 min. Trolox (0.1–1.5 mM) was used as a reference antioxidant ($R^2 = 0.9976$). A control was prepared with the same volume of ethanol without test compounds or reference antioxidant. ABTS·+ scavenging activity of the samples was expressed in millimoles Trolox (mM Trolox). Measurements were performed in triplicate.

Voltametric measurements. Stock standard solutions of compounds 1–9 ($c = 0.01 \text{ mol dm}^{-3}$) were prepared from dry pure substances in acetonitrile (CH₃CN, p.a. Kemika, Zagreb). For the supporting electrolyte, analytical-grade Et₄NClO₄ (Merck, Darmstadt, Germany) was used. Voltametric measurements were carried out using the computer-controlled electrochemical system "PGSTAT 101" (Eco Chemie, Utrecht, The Netherlands), controlled using the electrochemical software "NOVA 1.11". A three-electrode system (BioLogic, Claix, France) with a glassy carbon electrode (GCE) of 3 mm in diameter as a working electrode, Ag/Ag⁺ (0.01 M AgNO₃ in CH₃CN) as a reference electrode and a platinum wire as a counter electrode was used. All potentials were expressed versus the Ag/Ag⁺ (0.01 M AgNO₃) reference electrode. Before each run, the glassy carbon working electrode was polished with diamond suspension in spray (grain size 6 µm) and rinsed with ethanol and deionized water. The supporting electrolyte (0.1 M Et₄NClO₄ in CH₃CN) was placed in the electrochemical cell, and the required aliquot of the standard analyte solution was added. Before each experiment, the solution in the electrochemical cell was first degassed with high-purity nitrogen for 5 min, and the nitrogen blanket was maintained thereafter. All experiments were performed at room temperature. The presented results are reported as the mean value of three independent measurements. Cyclic voltammograms were taken in the potential range from -0.6 to 1.4 V.

4. Conclusions

We investigated the structure as well as the pattern of intramolecular hydrogen bonding in peptides containing three different ferrocene scaffolds, Fcd [-CO-Fn-CO-(II)], Fca [-CO-Fn-NH-(IV)], and Fcda [-NH-Fn-NH-(VI)], and the hydrophobic amino acids Val, Leu, and Phe by measuring concentration-dependent IR and NMR spectra, temperature-dependent NMR spectra, CD spectra, and the etitration of NMR and CD samples with DMSO.

The main conclusion from this study is that the hydrogen-bond-donating or accepting capacity of ferrocene scaffold influence the hydrogen bonding pattern more than bulkiness of the amino acid side chain. Conformational analysis revealed that the peptides derived from the hydrogen-bond-donating ferrocene-1,1'-diamine scaffold -NH-Fn-NH-(7-9) adopt the most ordered chiral arrangement based on the strongest intramolecular hydrogen bonds. Among the tested peptides, the most pronounced antioxidant activity determined

using the ABTS method exhibited conjugates (4–6) derived from the -CO-Fn-NH-, while MeO-Phe- $\underline{CO-Fn-CO}$ -Phe-OMe (3) had the highest antioxidant activity, as determined using the DPPH method.

Voltametric analysis revealed that the oxidation of peptide derivatives of ferrocene was influenced by the ferrocene scaffold, showing that peptides **VI** (7–9) with a ferrocene diamine scaffold (-NH–Fn–NH-) require lower potential than peptides **IV** (4–6) and **II** (1–3) with -CO–Fn–NH- and -CO–Fn–CO- scaffold, respectively; which may also contribute to their antioxidant properties. However, the most effective ABTS⁺ radical quenchers were peptides with a -CO–Fn–NH- scaffold (group **IV**, i.e., with moderately low oxidation potential, implying that the scavenging activity of compounds 1–9 is not mainly governed by their susceptibility to oxidation).

Supplementary Materials: The following supporting information can be downloaded at: https:// www.mdpi.com/article/10.3390/inorganics12070195/s1. Figures S1-S49: Figure S1. The NH stretching vibrations in concentration-dependent IR spectra of 1–9 in DCM [CH₂Cl₂, (—) $c = 5 \times 10^{-2}$ M]; Figure S2. Cotton effects of **1–9** {CH₂Cl₂ [(—) $c = 5 \times 10^{-3}$ M), CH₂Cl₂ ($c = 5 \times 10^{-3}$ M) containing 20% of DMSO (···)}; Figure S3. The NH stretching vibrations in concentration-dependent IR spectra of 1 in DCM (CH₂Cl₂, [(—) $c = 5 \times 10^{-2}$ M, (—) $c = 2.5 \times 10^{-2}$ M, (—) $c = 1.25 \times 10^{-2}$ M, (—) c = 6.13×10^{-3} M, (—) $c = 3 \times 10^{-3}$ M]; Figure S4. Cotton effect of 1 {CH₂Cl₂ [(—) $c = 5 \times 10^{-3}$ M), CH_2Cl_2 ($c = 5 \times 10^{-3}$ M) containing 20% of DMSO (···)}; Figure S5. Concentration-dependent NH chemical shifts of compound 1 in CDCl₃; Figure S6. Temperature-dependent NH chemical shifts of compound 1 ($c = 2.5 \times 10^{-2}$ M); Figure S7. ¹H NMR spectra of compound 1 at varying concentrations of DMSO in CDCl₃ ($c = 2.5 \times 10^{-2}$ M); Figure S8. The NH stretching vibrations in concentrationdependent IR spectra of 2 in DCM (CH₂Cl₂, [(—) $c = 5 \times 10^{-2}$ M, (—) $c = 2.5 \times 10^{-2}$ M, (—) c = 1.25×10^{-2} M, (—) $c = 6.13 \times 10^{-3}$ M, (—) $c = 3 \times 10^{-3}$ M]; Figure S9. Cotton effect of 2 {CH₂Cl₂ [(—) $c = 5 \times 10^{-3}$ M), CH₂Cl₂ ($c = 5 \times 10^{-3}$ M) containing 20% of DMSO (···)}; Figure S10. Concentrationdependent NH chemical shifts of compound 2 in CDCl₃; Figure S11. Temperature-dependent NH chemical shifts of compound 2 ($c = 2.5 \times 10^{-2}$ M); Figure S12. ¹H NMR spectra of compound 2 at varying concentrations of DMSO in CDCl₃ ($c = 2.5 \times 10^{-2}$ M); Figure S13. The NH stretching vibrations in concentration-dependent IR spectra of 3 in DCM (CH₂Cl₂, [(—) $c = 5 \times 10^{-2}$ M, (—)c= 2.5×10^{-2} M, (—) $c = 1.25 \times 10^{-2}$ M, (—) $c = 6.13 \times 10^{-3}$ M, (—) $c = 3 \times 10^{-3}$ M]; Figure S14. Cotton effect of 3 {CH₂Cl₂ [(—) $c = 5 \times 10^{-3}$ M), CH₂Cl₂ ($c = 5 \times 10^{-3}$ M) containing 20% of DMSO (···)}; Figure S15. Concentration-dependent NH chemical shifts of compound 3 in CDCl₃; Figure S16. Temperature-dependent NH chemical shifts of compound 3 ($c = 2.5 \times 10^{-2}$ M); Figure S17. ¹H NMR spectra of compound 3 at varying concentrations of DMSO in CDCl₃ ($c = 2.5 \times 10^{-2}$ M); Figure S18. The NH stretching vibrations in concentration-dependent IR spectra of 4 in DCM (CH_2Cl_2 , [(—)c = $5 \times 10^{-2} \,\mathrm{M}$, (—) $c = 2.5 \times 10^{-2} \,\mathrm{M}$, (—) $c = 1.25 \times 10^{-2} \,\mathrm{M}$, (—) $c = 6.13 \times 10^{-3} \,\mathrm{M}$, (—) $c = 3 \times 10^{-3} \,\mathrm{M}$]; Figure S19. Cotton effect of 4 {CH₂Cl₂ [(—) $c = 5 \times 10^{-3}$ M), CH₂Cl₂ ($c = 5 \times 10^{-3}$ M) containing 20% of DMSO (···)}; Figure S20. Concentration-dependent NH chemical shifts of compound 4 in CDCl₃; Figure S21. Temperature-dependent NH chemical shifts of compound 4 ($c = 2.5 \times 10^{-2}$ M); Figure S22. ¹H NMR spectra of compound 4 at varying concentrations of DMSO in CDCl₃ (c = 2.5×10^{-2} M); Figure S23. The NH stretching vibrations in concentration-dependent IR spectra of 5 in DCM (CH₂Cl₂, [(—) $c = 5 \times 10^{-2}$ M, (—) $c = 2.5 \times 10^{-2}$ M, (—) $c = 1.25 \times 10^{-2}$ M, (—) $c = 6.13 \times 10^{-3} \text{ M}$, (—) $c = 3 \times 10^{-3} \text{ M}$; Figure S24. Cotton effect of 5 {CH₂Cl₂ [(—) c = 5×10^{-3} M), CH₂Cl₂ ($c = 5 \times 10^{-3}$ M) containing 20% of DMSO (···)}; Figure S25. Concentrationdependent NH chemical shifts of compound 5 in CDCl₃; Figure S26. Temperature-dependent NH chemical shifts of compound 5 ($c = 2.5 \times 10^{-2}$ M); Figure S27. ¹H NMR spectra of compound 5 at varying concentrations of DMSO in CDCl₃ ($c = 2.5 \times 10^{-2}$ M); Figure S28. The NH stretching vibrations in concentration-dependent IR spectra of 6 in DCM (CH₂Cl₂, [(—) $c = 5 \times 10^{-2}$ M, (—)c= 2.5×10^{-2} M, (—) $c = 1.25 \times 10^{-2}$ M, (—) $c = 6.13 \times 10^{-3}$ M, (—) $c = 3 \times 10^{-3}$ M]; Figure S29. Cotton effect of 6 {CH₂Cl₂ [(—) $c = 5 \times 10^{-3}$ M), CH₂Cl₂ ($c = 5 \times 10^{-3}$ M) containing 20% of DMSO (···)}; Figure S30. Concentration-dependent NH chemical shifts of compound 6 in CDCl₃; Figure S31. Temperature-dependent NH chemical shifts of compound 6 ($c = 2.5 \times 10^{-2}$ M); Figure S32. ¹H NMR spectra of compound 6 at varying concentrations of DMSO in CDCl₃ ($c = 2.5 \times 10^{-2}$ M); Figure S33. The NH stretching vibrations in concentration-dependent IR spectra of 7 in DCM (CH_2Cl_2 , [(—)c = $5 \times 10^{-2} \,\mathrm{M}$, (—) $c = 2.5 \times 10^{-2} \,\mathrm{M}$, (—) $c = 1.25 \times 10^{-2} \,\mathrm{M}$, (—) $c = 6.13 \times 10^{-3} \,\mathrm{M}$, (—) $c = 3 \times 10^{-3} \,\mathrm{M}$];

Figure S34. Cotton effect of 7 {CH₂Cl₂ [(—) $c = 5 \times 10^{-3}$ M), CH₂Cl₂ ($c = 5 \times 10^{-3}$ M) containing 20% of DMSO (···)}; Figure S35. Concentration-dependent NH chemical shifts of compound 7 in CDCl₃; Figure S36. Temperature-dependent NH chemical shifts of compound 7 ($c = 2.5 \times 10^{-2}$ M); Figure S37. ¹H NMR spectra of compound 7 at varying concentrations of DMSO in CDCl₃ (c = 2.5×10^{-2} M); Figure S38. The NH stretching vibrations in concentration-dependent IR spectra of 8 in DCM (CH₂Cl₂, [(—) $c = 5 \times 10^{-2}$ M, (—) $c = 2.5 \times 10^{-2}$ M, (—) $c = 1.25 \times 10^{-2}$ M, (—) c = $6.13 \times 10^{-3} \text{ M}$, (—) $c = 3 \times 10^{-3} \text{ M}$; Figure S39. Cotton effect of 8 {CH₂Cl₂ [(—) $c = 5 \times 10^{-3} \text{ M}$), CH_2Cl_2 ($c = 5 \times 10^{-3}$ M) containing 20% of DMSO (···)}; Figure S40. Concentration-dependent NH chemical shifts of compound 8 in CDCl₃; Figure S41. Temperature-dependent NH chemical shifts of compound 8 ($c = 2.5 \times 10^{-2}$ M); Figure S42. ¹H NMR spectra of compound 8 at varying concentrations of DMSO in CDCl₃ ($c = 2.5 \times 10^{-2}$ M); Figure S43. The NH stretching vibrations in concentration-dependent IR spectra of 9 in DCM (CH₂Cl₂, [(—) $c = 5 \times 10^{-2}$ M, (—)c = 2.5×10^{-2} M, (—) $c = 1.25 \times 10^{-2}$ M, (—) $c = 6.13 \times 10^{-3}$ M, (—) $c = 3 \times 10^{-3}$ M]; Figure S44. Cotton effect of 9 {CH₂Cl₂ [(—) $c = 5 \times 10^{-3}$ M), CH₂Cl₂ ($c = 5 \times 10^{-3}$ M) containing 20% of DMSO (···)}; Figure S45. Concentration-dependent NH chemical shifts of compound 9 in CDCl₃; Figure S46. Temperature-dependent NH chemical shifts of compound 9 ($c = 2.5 \times 10^{-2}$ M); Figure S47. ¹H NMR spectra of compound 9 at varying concentrations of DMSO in CDCl₃ ($c = 2.5 \times 10^{-2}$ M).

Author Contributions: Conceptualization. M.K., S.R., D.J. and J.M.; methodology. L.B., M.K. and J.M.; validation. M.Č.S., K.H.Č. and S.R.; formal analysis. M.K., S.R., K.H.Č. and D.J.; investigation. M.K., S.R., K.H.Č., D.J. and M.Č.S.; resources. L.B.; writing—original draft preparation. M.K. and J.M.; writing—review and editing. L.B., S.R., M.Č.S. and D.J.; visualization. M.K.; supervision. L.B.; project administration. L.B.; funding acquisition. L.B. All authors have read and agreed to the published version of the manuscript.

Funding: This work has been fully supported by the Croatian Science Foundation under the project IP-2020-02-9162.

Data Availability Statement: The spectroscopic and biological evaluation data are provided as figures and tables and are included in this paper.

Conflicts of Interest: The authors declare no conflict of interest.

References

- 1. Dias, C.L.; Karttunen, M.; Chan, H.S. Hydrophobic interactions in the formation of secondary structures in small peptides. *Phys. Rev. E* **2011**, *84*, 041931. [CrossRef]
- 2. Xiong, H.; Buckwalter, B.L.; Shieh, H.-M.; Hecht, M.H. Periodicity of polar and nonpolar amino acids is the major determinant of secondary structure in self-assembling oligomeric peptides. *Proc. Natl. Acad. Sci. USA* 1995, 92, 6349–6353. [CrossRef] [PubMed]
- 3. Dill, K.A. Dominant forces in protein folding. *Biochemistry* 1990, 29, 7133–7155. [CrossRef]
- 4. Nowick, J.S. Exploring β-Sheet Structure and Interactions with Chemical Model Systems. *Acc. Chem. Res.* **2008**, *41*, 1319–1330. [CrossRef] [PubMed]
- 5. Kovačević, M.; Kodrin, I.; Cetina, M.; Kmetič, I.; Murati, T.; Čakić-Semenčić, M.; Roca, S.; Barišić, L. The conjugate of β-turn-nucleating ferrocene-1,1′-diamine and amino acids. A novel synthetic approach and conformational analysis. *Dalton Trans.* **2015**, 44, 16405–16420. [CrossRef] [PubMed]
- 6. Van Staveren, D.R.; Weyhermüller, T.; Metzler-Nolte, N. Organometallic β-turn mimetics. A structural and spectroscopic study of inter-strand hydrogen bonding in ferrocene and cobaltocenium conjugates of amino acids and dipeptides. *Dalton Trans.* **2003**, *2*, 210–220. [CrossRef]
- Čakić Semenčić, M.; Kodrin, I.; Molčanov, K.; Kovačević, M.; Rapić, V. Novel ferrocene imide derivatives: Synthesis, conformational analysis and X-ray structure. Heliyon 2022, 8, e09470. [CrossRef]
- 8. Moriuchi, T.; Ohmura, S.D.; Moriuchi-Kawakami, T. Chirality Induction in Bioorganometallic Conjugates. *Inorganics* **2018**, *6*, 111. [CrossRef]
- 9. Kirin, S.I.; Kraatz, H.B.; Metzler-Nolte, N. Systematizing structural motifs and nomenclature in 1,n'-disubstituted ferrocene peptides. *Chem. Soc. Rew.* **2006**, 35, 348–354. [CrossRef]
- 10. Herrick, R.S.; Jarret, R.M.; Curran, T.P.; Dragoli, D.R.; Flaherty, M.B.; Lindyberg, S.E.; Slate, R.A.; Thornton, L.C. Ordered conformations in bis(amino acid) derivatives of 1,1'-ferrocenedicarboxylic acid. *Tetrahedron Lett.* 1996, 37, 5289–5292. [CrossRef]
- 11. Xu, Y.; Saweczko, P.; Kraatz, H.-B. 1,1'-Ferrocenoyl-oligoprolines. A synthetic, structural and electrochemical study. *J. Organomet. Chem.* **2001**, 637, 335–342. [CrossRef]
- 12. Moriuchi, T.; Hirao, T. Dipeptide-induced chirality organization. J. Incl. Phenom. Macrocycl. Chem. 2012, 74, 23–40. [CrossRef]
- 13. Moriuchi, T.; Hirao, T. Design of ferrocene-dipeptide bioorganometallic conjugates to induce chirality-organized structures. *Acc. Chem. Res.* **2010**, *43*, 1040–1051. [CrossRef] [PubMed]

14. Barišić, L.; Čakić, M.; Mahmoud, K.A.; Liu, Y.-N.; Kraatz, H.-B.; Pritzkow, H.; Kirin, S.I.; Metzler-Nolte, N.; Rapić, V. Helically Chiral Ferrocene Peptides Containing 1'-Aminoferrocene-1-Carboxylic Acid Subunits as Turn Inducers. *Chem. Eur. J.* **2006**, *12*, 4965–4980. [CrossRef] [PubMed]

- 15. Čakić Semenčić, M.; Siebler, D.; Heinze, K.; Rapić, V. Bis- and Trisamides Derived From 1'-Aminoferrocene-1-carboxylic Acid and α-Amino Acids: Synthesis and Conformational Analysis. *Organometallics* **2009**, *28*, 2028–2037. [CrossRef]
- 16. Kovačević, M.; Molčanov, K.; Radošević, K.; Srček Gaurina, V.; Roca, S.; Čače, A.; Barišić, L. Conjugates of 1'-aminoferrocene-1-carboxylic acid and proline: Synthesis, conformational analysis and biological evaluation. *Molecules* **2014**, *21*, 12852–12880. [CrossRef] [PubMed]
- 17. Kovačević, M.; Čakić Semenčić, M.; Radošević, K.; Molčanov, K.; Roca, S.; Šimunović, L.; Kodrin, I.; Barišić, L. Conformational Preferences and Antiproliferative Activity of Peptidomimetics Containing Methyl 1'-Aminoferrocene-1-carboxylate and Turn-Forming Homo- and Heterochiral Pro-Ala Motifs. *Int. J. Mol. Sci.* 2021, 22, 13532. [CrossRef] [PubMed]
- Kovačević, M.; Kodrin, I.; Roca, S.; Molčanov, K.; Shen, Y.; Adhikari, B.; Kraatz, H.B.; Barišić, L. Helically Chiral Peptides That Contain Ferrocene-1,1'-diamine Scaffolds as a Turn Inducer. Chem. Eur. J. 2017, 23, 10372–10395. [CrossRef] [PubMed]
- 19. Chowdhury, S.; Mahmoud, K.A.; Schatte, G.; Kraatz, H.-B. Amino acid conjugates of 1,1'-diaminoferrocene. Synthesis and chiral organization. *Org. Biomol. Chem.* **2005**, *3*, 3018–3023. [CrossRef]
- Kovačević, M.; Markulin, D.; Zelenika, M.; Marjanović, M.; Lovrić, M.; Polančec, D.; Ivančić, M.; Mrvčić, J.; Molčanov, K.; Milašinović, V.; et al. Hydrogen Bonding Drives Helical Chirality via 10-Membered Rings in Dipeptide Conjugates of Ferrocene-1,1'-Diamine. Int. J. Mol. Sci. 2022, 23, 12233. [CrossRef]
- 21. Astruc, D. Why is Ferrocene so Exceptional? Eur. J. Inorg. Chem. 2017, 2017, 6–29. [CrossRef]
- 22. Patra, M.; Gasser, G. The medicinal chemistry of ferrocene and its derivatives. Nat. Rev. Chem. 2017, 1, 0066. [CrossRef]
- 23. Ludwig, B.S.; Correia, J.D.G.; Kühn, F.E. Ferrocene derivatives as anti-infective agents. *Coord. Chem. Rev.* **2019**, *396*, 22–48. [CrossRef]
- 24. Sharma, B.; Kumar, V. Has Ferrocene Really Delivered Its Role in Accentuating the Bioactivity of Organic Scaffolds? *J. Med. Chem.* **2021**, *64*, 16865–16921. [CrossRef]
- 25. Mueller, L.K.; Baumruck, A.C.; Zhdanova, H.; Tietze, A.A. Challenges and Perspectives in Chemical Synthesis of Highly Hydrophobic Peptides. *Front. Bioeng. Biotechnol.* **2020**, *8*, 162. [CrossRef]
- Borrelli, A.; Tornesello, A.L.; Tornesello, M.L.; Buonaguro, F.M. Cell Penetrating Peptides as Molecular Carriers for Anti-Cancer Agents. *Molecules* 2018, 23, 295. [CrossRef]
- 27. Blaber, M.; Zhang, X.J.; Matthews, B.W. Structural Basis of Amino Acid α Helix Propensity. *Science* **1993**, 260, 1637–1640. [CrossRef]
- 28. Saravanan, R.; Li, X.; Lim, K.; Mohanram, H.; Peng, L.; Mishra, B.; Basu, A.; Lee, J.M.; Bhattacharjya, S.; Leong, S.S. Design of short membrane selective antimicrobial peptides containing tryptophan and arginine residues for improved activity, salt-resistance, and biocompatibility. *Biotechnol. Bioeng.* 2014, 111, 37–49. [CrossRef] [PubMed]
- 29. Saint Jean, K.D.; Henderson, K.D.; Chrom, C.L.; Abiuso, L.E.; Renn, L.M.; Caputo, G.A. Effects of Hydrophobic Amino Acid Substitutions on Antimicrobial Peptide Behavior. *Probiotics Antimicrob. Prot.* **2018**, *10*, 408–419. [CrossRef]
- 30. Zou, T.-B.; He, T.-P.; Li, H.-B.; Tang, H.-W.; Xia, E.-Q. The Structure-Activity Relationship of the Antioxidant Peptides from Natural Proteins. *Molecules* **2016**, *21*, 72. [CrossRef]
- 31. Wang, B.; Gong, Y.D.; Li, Z.R.; Yu, D.; Chi, C.F.; Ma, J.Y. Isolation and characterisation of five novel antioxidant peptides from ethanol-soluble proteins hydrolysate of spotless smoothhound (*Mustelus griseus*) muscle. *J. Funct. Foods* **2014**, *6*, 176–185. [CrossRef]
- 32. Ren, Y.; Wu, H.; Li, X.; Lai, F.; Xiao, X. Purification and characterization of high antioxidant peptides from duck egg white protein hydrolysates. *Biochem. Biophys. Res. Commun.* **2014**, 452, 888–894. [CrossRef] [PubMed]
- 33. Chanput, W.; Nakai, S.; Theerakulkait, C. Introduction of new computer softwares for classification and prediction purposes of bioactive peptides: Case study in antioxidative tripeptides. *Int. J. Food Prop.* **2010**, *13*, 947–959. [CrossRef]
- 34. Li, Y.-W.; Li, B.; He, J.; Qian, P. Structure-activity relationship study of antioxidative peptides by QSAR modeling: The amino acid next to C-terminus affects the activity. *J. Pept. Sci.* **2011**, *17*, 454–462. [CrossRef] [PubMed]
- 35. Li, Y.-W.; Li, B.; He, J.; Qian, P. Quantitative structureactivity relationship study of antioxidative peptide by using different sets of amino acids descriptors. *J. Mol. Struct.* **2011**, *998*, 53–61. [CrossRef]
- 36. Ohashi, Y.; Onuma, R.; Naganuma, T.; Ogawa, T.; Naude, R.; Nokihara, K.; Muramoto, K. Antioxidant properties of tripeptides revealed by a comparison of six different assays. *Food Sci. Technol. Res.* **2015**, *21*, 695–704. [CrossRef]
- 37. Saidi, S.; Deratani, A.; Belleville, M.P.; Amar, R.B. Antioxidant properties of peptide fractions from tuna dark muscle protein by-product hydrolysate produced by membrane fractionation process. *Food Res. Int.* **2014**, *65*, 329–336. [CrossRef]
- 38. Kovačević, M.; Čakić Semenčić, M.; Kodrin, I.; Roca, S.; Perica, J.; Mrvčić, J.; Stanzer, D.; Molčanov, K.; Milašinović, V.; Brkljačić, L. Biological Evaluation and Conformational Preferences of Ferrocene Dipeptides with Hydrophobic Amino Acids. *Inorganics* 2023, 11, 29. [CrossRef]
- 39. Galka, M.M.; Kraatz, H.-B. Electron Transfer Studies on Self-Assembled Monolayers of Helical Ferrocenoyl-Oligoproline-Cystamine Bound to Gold. *Chem. Phys. Chem.* **2002**, *3*, 356–359. [CrossRef]
- 40. Huang, H.; Mu, L.; He, J.; Cheng, J.-P. Ferrocenyl-Bearing Cyclopseudopeptides as Redox-Switchable Cation Receptors. *J. Org. Chem.* **2003**, *68*, 7605–7611. [CrossRef]

41. Kong, J.; Yu, S. Fourier transform infrared spectroscopic analysis of protein secondary structures. *Acta Biochim. Biophys. Sin.* **2007**, 39, 549–559. [CrossRef] [PubMed]

- 42. Ganesh, S.; Jayakumar, R. Role of *N-t*-Boc group in helix initiation in a novel tetrapeptide. *J. Peptide Res.* **2002**, *59*, 249–256. [CrossRef] [PubMed]
- 43. Pardi, A.; Wagner, G.; Wuthrich, K. Protein conformation and proton nuclear-magnetic-resonance chemical shifts. *Eur. J. Biochem.* 1983, 137, 445–454. [CrossRef] [PubMed]
- 44. Gellman, S.H.; Dado, G.P.; Liang, G.-B.; Adams, B.R. Conformation-directing effects of a single intramolecular amide-amide hydrogen bond: Variable-temperature NMR and IR studies on a homologous diamide series. *J. Am. Chem. Soc.* **1991**, 113, 1164–1173. [CrossRef]
- 45. Baxter, N.J.; Williamson, M.P. Temperature dependence of ¹H chemical shifts in proteins. *J. Biomol. NMR* **1997**, *9*, 359–369. [CrossRef] [PubMed]
- 46. Liu, J.-Y.; Sun, X.-Y.; Tang, Q.; Song, J.-J.; Li, X.-Q.; Gong, B.; Liu, R.; Lu, Z.-L. An unnatural tripeptide structure containing intramolecular double H-bond mimics a turn-hairpin conformation. *Org. Biomol. Chem.* **2021**, *19*, 4359–4363. [CrossRef] [PubMed]
- 47. Berger, N.; Wollny, L.J.B.; Sokkar, P.; Mittal, S.; Mieres-Perez, J.; Stoll, R.; Sander, W.; Sanchez-Garcia, E. Solvent-Enhanced Conformational Flexibility of Cyclic Tetrapeptides. *ChemPhysChem* **2019**, 20, 1664–1670. [CrossRef] [PubMed]
- 48. Stevens, E.S.; Sugawara, N.; Bonora, G.M.; Toniolo, C. Conformational analysis of linear peptides. 3. Temperature dependence of NH chemical shifts in chloroform. *J. Am. Chem. Soc.* **1980**, *102*, 7048–7050. [CrossRef]
- 49. Sladojevich, F.; Guarna, A.; Trabocchi, A. Evaluation of stereochemically dense morpholine-based scaffolds as proline surrogates in β-turn peptides. *Org. Biomol. Chem.* **2010**, *8*, 916–924. [CrossRef]
- 50. Curran, T.P.; Marques, K.A.; Silva, M.V. Bis(amino acid) derivatives of 1,4-diamino2-butyne that adopt a *C*₂-symmetric turn conformation. *Org. Biomol. Chem.* **2005**, *3*, 4134–4138. [CrossRef]
- 51. Kovač, V.; Čakić Semenčić, M.; Kodrin, I.; Roca, S.; Rapić, V. Ferrocene-dipeptide conjugates derived from aminoferrocene and 1-acetyl-1'-aminoferrocene: Synthesis and conformational studies. *Tetrahedron* **2013**, *69*, 10497–10506. [CrossRef]
- 52. Pignataro, M.F.; Herrera, M.G.; Dodero, V.I. Evaluation of Peptide/Protein Self-Assembly and Aggregation by Spectroscopic Methods. *Molecules* **2020**, 25, 4854. [CrossRef] [PubMed]
- 53. Rogers, D.M.; Jasim, S.B.; Dyer, N.T.; Auvray, F.; Réfrégiers, M.; Hirst, J.D. Electronic Circular Dichroism Spectroscopy of Proteins. *Chem* **2019**, *5*, 2751–2774. [CrossRef]
- 54. Moriuchi, T. Helical Chirality of Ferrocene Moieties in Cyclic Ferrocene-Peptide Conjugates. *Chem. Eur. J.* **2022**, 2022, e202100902. [CrossRef]
- 55. Ternansky, R.J.; Draheim, S.E.; Pike, A.J.; Counter, F.T.; Eudaly, J.A.; Kasher, J.S. Structure-activity relationship within a series of pyrazolidinone antibacterial agents. 2. Effect of side-chain modification on in vitro activity and pharmacokinetic parameters. *J. Med. Chem.* 1993, 36, 3224–3229. [CrossRef] [PubMed]
- 56. Bugarinović, J.; Pešić, M.; Minić, A.; Katanić Stanković, J.; Ilic Komatina, D.; Pejovic, A.; Mihailovic, V.; Stevanović, D.; Nastasijevic, B.; Damljanović, I. Ferrocene-containing tetrahydropyrazolopyrazolopes: Antioxidant and antimicrobial activity. *J. Inorg. Biochem.* **2018**, *189*, 134–142. [CrossRef] [PubMed]
- 57. Milaeva, E.R.; Filimonova, S.I.; Meleshonkova, N.N.; Dubova, L.G.; Shevtsova, E.F.; Bachurin, S.O.; Zefirov, N.S. Antioxidative Activity of Ferrocenes Bearing 2,6-Di-Tert-Butylphenol Moieties. *Bioinorg. Chem. Appl.* 2010, 2010, 165482. [CrossRef] [PubMed]
- 58. Liu, Z.Q. Enhancing Antioxidant Effect against Peroxyl Radical-induced Oxidation of DNA: Linking with Ferrocene Moiety! *Chem. Rec.* **2019**, *19*, 2385–2396. [CrossRef]
- 59. Minić Jančić, A.; Katanić Stanković, J.S.; Srećković, N.; Mihailović, V.; Ilić Komatina, D.; Stevanović, D. Ferrocene-containing tetrahydropyrimidin-2(1H)-ones: Antioxidant and antimicrobial activity. *J. Organomet. Chem.* **2022**, *967*, 122335. [CrossRef]
- 60. Tabrizi, L.; Nguyen, T.L.A.; Tran, H.D.T.; Pham, M.K.; Dao, D.Q. Antioxidant and Anticancer Properties of Functionalized Ferrocene with Hydroxycinnamate Derivatives-An Integrated Experimental and Theoretical Study. *J. Chem. Inf. Model.* **2020**, *60*, 6185–6203. [CrossRef]
- 61. Santi, S.; Biondi, B.; Cardena, R.; Bisello, A.; Schiesari, R.; Tomelleri, S.; Crisma, M.; Formaggio, F. Helical versus Flat Bis-Ferrocenyl End-Capped Peptides: The Influence of the Molecular Skeleton on Redox Properties. *Molecules* **2022**, 27, 6128. [CrossRef]
- 62. Biondi, B.; Bisello, A.; Cardena, R.; Schiesari, R.; Facci, M.; Cerveson, L.; Rancan, M.; Formaggio, F.; Santi, S. Conformational Analysis and Through-Chain Charge Propagation in Ferrocenyl-Conjugated Homopeptides of 2,3-Diaminopropionic acid (Dap). *Eur. J. Inorg. Chem.* 2022, 2022, e202100. [CrossRef]
- 63. Rodrigues Pontiha, A.D.; Alves Jorge, S.M.; Chiorcea-Paquim, A.M.; Diculescu, V.C.; Oliveira-Brett, A.M. In situ evaluation of anticancer drug methotrexate-DNA interaction using a DNA-electrochemical biosensor and AFM characterization. *Phys. Chem. Phys.* **2011**, *13*, 5227–5234. [CrossRef]
- 64. Chiorcea-Paquim, A.M.; Rodrigues Pontiha, A.D.; Oliveira-Brett, A.M. Quadruplex-targeting anticancer drug BRACO-19 voltammetric and AFM characterization. *Electrochim. Acta* **2015**, 174, 155–163. [CrossRef]
- 65. Diculescu, V.C.; Oliveira-Brett, A.M. In situ electrochemical evaluation of dsDNA interaction with the anticancer drug danusertib nitrenium radical product using the DNA-electrochemical biosensor. *Bioelectrochemistry* **2016**, 107, 50–57. [CrossRef]
- 66. Novak Jovanović, I.; Komorsky-Lovrić, Š.; Lucić Vrdoljak, A.; Popović, A.R.; Neuberg, M. Voltammetric characterisation of anticancer drug irinotecan. *Electroanalysis* **2018**, *30*, 336–344. [CrossRef]

67. Bond, A.M.; McLennan, E.A.; Stojanovic, R.S.; Thomas, F.G. Assessment of conditions under which the oxidation of ferrocene can be used as a standard voltammetric reference process in aqueous media. *Anal. Chem.* **1987**, *59*, 2853–2860. [CrossRef]

- 68. Neghmouche, N.S.; Khelef, A.; Lanez, T. Electrochemistry characterization of ferrocene/ferricenium redox couple at glassy carbon electrode. *J. Fundam. Appl. Sci.* **2009**, *1*, 23–30. [CrossRef]
- 69. Batterjee, S.M.; Marzouk, M.I.; Aazab, M.E.; El-Hashash, M.A. The Electrochemistry of Some Ferrocene Derivatives: Redox Potential and Substituent Effects. *Appl. Organomet. Chem.* **2003**, *17*, 291–297. [CrossRef]
- 70. Rep, V.; Piškor, M.; Šimek, H.; Mišetić, P.; Grbčić, P.; Padovan, J.; Gabelica Marković, V.; Jadreško, D.; Pavelić, K.; Kraljević Pavelić, S.; et al. Purine and Purine Isostere Derivatives of Ferrocene: An Evaluation of ADME, Antitumor and Electrochemical Properties. *Molecules* **2020**, 25, 1570. [CrossRef]
- 71. Adenier, A.; Chehimi, M.M.; Gallardo, I.; Pinson, J.; Vila, N. Electrochemical Oxidation of Aliphatic Amines and Their Attachment to Carbon and Metal Surfaces. *Langmuir* **2004**, *20*, 8243–8253. [CrossRef] [PubMed]
- 72. Brand-Williams, W.; Cuvelier, M.E.; Berset, C. Use of a Free Radical Method to Evaluate Antioxidant Activity. *LWT* **1995**, 28, 25–30. [CrossRef]
- 73. Re, R.; Pellegrini, N.; Proteggente, A.; Pannala, A.; Yang, M.; Rice-Evans, C. Antioxidant activity applying an improved ABTS radical cation decolorization assay. *Free Radic. Biol. Med.* 1999, 26, 1231–1237. [CrossRef] [PubMed]

Disclaimer/Publisher's Note: The statements, opinions and data contained in all publications are solely those of the individual author(s) and contributor(s) and not of MDPI and/or the editor(s). MDPI and/or the editor(s) disclaim responsibility for any injury to people or property resulting from any ideas, methods, instructions or products referred to in the content.